
Scalable Machines with Intrinsic Higher Mental-State Dynamics

Ahsan Adeel*¹ M. Bilal¹

TREND Project: github.com/ARIA-Funded-TREND/IHMS

Drawing on recent breakthroughs in cellular neurobiology and detailed biophysical modeling linking neocortical pyramidal neurons to distinct mental-state regimes, this work introduces a mathematically grounded formulation showing how models (e.g., Transformers) can implement computational principles underlying awake imaginative thought to pre-select relevant information before attention is applied via triadic modulation loops among queries (Q), keys (K), and values (V). Scalability experiments on ImageNet-1K, benchmarked against a standard Vision Transformer (ViT), demonstrate significantly faster learning with reduced computational demand (fewer heads, layers, and tokens), consistent with our prior findings in reinforcement learning and language modeling. The approach operates at approximately $O(N)$ complexity with respect to the number of input tokens N .

1. Introduction

Attending to what is relevant is fundamental to both the mammalian brain and machine learning models. Yet determining relevance remains a core challenge. Modern artificial neural networks, such as Transformer models (Vaswani et al., 2017) and their variants, compute relevance through attention over learned Q , K , and V representations. However, these representations are largely treated as unconstrained learned features and lack intrinsic predictive mechanisms during the feedforward (FF) phase to evaluate whether they are coherent, consistent, contextually appropriate, or even relevant prior to attention.

Recent cellular neurobiology (Larkum et al., 1999; Aru et al., 2021; Phillips et al., 2024; Storm et al., 2024) and detailed biophysical modeling (Graham et al., 2025) provide a contrasting mechanism. In the mammalian neocortex, layer 5 pyramidal two-point neurons (TPNs) (Figure 1(a)) integrate two distinct input streams: FF sensory evidence (receptive

field; RF¹, denoted R) arriving at basal dendrites, and contextual input (contextual field; CF², denoted C) arriving at apical dendrites. When basal and apical compartments are simultaneously depolarized, TPNs generate brief high-frequency bursts, signaling coherence between evidence and context. This bursting minimizes predictive error, or free energy (Friston, 2010), by selectively amplifying relevant information while suppressing irrelevant signals (Marvan & Phillips, 2024), enabling context-sensitive processing before attention.

Bursting probability depends on the relative strengths of R (evidence) and C (context) inputs and varies systematically across processing regimes associated with different mental states, including slow-wave (SW) sleep, wakefulness, and rapid eye movement (REM) sleep (Aru et al., 2021; Phillips et al., 2024; Storm et al., 2024). Four operational modes of neocortical pyramidal TPNs have been identified (Phillips et al., 2024; Graham et al., 2025):

(1) During typical wakefulness, apical dendrites (C), when receiving moderate input alongside high R input, amplify the transmission of FF basal or perisomatic input. This regime is termed *apical amplification (AA)*, in which bursting probability is primarily determined by R but modulated by C . Such context-sensitive cooperative amplification supports cognitive abilities while limiting internally generated imagery and thought.

(2) When C input is high and R input is low, apical input can independently drive axonal spiking output, a condition associated with REM sleep and internally generated thought (imagination). This regime is termed *apical drive (AD)*, in which bursting probability is largely determined by C alone.

(3) When both C and R inputs are high, bursting probability is maximal and is associated with imaginative cognition during wakefulness (awake thought); this regime is termed *AD + Awake*.

(4) When C input has no effect on the neuron’s current output, the state is associated with SW sleep and is termed *apical isolation (AI)*. See A.1–A.4 for further details.

¹TREND Project: Funded by the UK Advanced Research + Invention Agency (ARIA). Correspondence to: *Ahsan Adeel <ahsan.adeel1@stir.ac.uk>.

¹RF refers to the external world: the region of the sensory periphery where stimuli influence the electrical activity of sensory cells.

²CF refers to the internal world: signals from diverse cortical and subcortical sources, including feedback.

Inspired by these cellular mechanisms, we developed Cooperative Context-sensitive Cognitive Computation (Co⁴) (Adeel, 2025), an architecture that extends standard Transformer models. Co⁴ leverages internally generated mental-state dynamics, formulated as R - C interactions analogous to those described above (Phillips et al., 2024; Graham et al., 2025), to enable on-the-fly selection of relevant information prior to attention. These dynamics are implemented through triadic modulation loops among Q -, K -, and V -like populations modeled on TPNs and governed by modulatory (MOD) cooperation laws associated with mental-state regimes (Graham et al., 2025).

The MOD cooperation laws used here follow the qualitative structure of dendritic transfer functions reported in biophysical models of TPNs (Graham et al., 2025), where the functional form matters more than the exact analytic specification. They mirror nonlinear R - C interactions and represent bursting probability as a continuous amplitude reflecting the coherence between the R and C streams. This provides an empirically grounded basis for the proposed regime-dependent dynamics. These regimes, however, serve as operational descriptors and do not imply that Co⁴ possesses subjective experience or consciousness.

During triadic modulation, each TPN population treats its latent representation as the primary evidence stream (R), while receiving contextual input (C) from the other evolving populations. In Q-TPNs, latent Q is refined through contextual signals from evolving K , amplifying those Q elements coherent with K and progressively shaping a context-sensitive set of queries. Similarly, in K-TPNs, latent K is updated in response to evolving Q , selectively strengthening those K components aligned with the emerging query structure and refining the contextual representation. In V-TPNs, latent V is stabilized through interaction with the jointly updated Q and K , reinforcing values that are consistent with both evidence and contextual structure. Processing regimes for individual Q-, K-, and V-TPNs shift between AA, AD, and AD + Awake depending on the relative strengths of R and C inputs.

Once Co⁴ establishes coherence, i.e., separates coherent (relevant) from incoherent (irrelevant) Q-K-V token representations, the exact downstream readout operator (e.g., pruning, gating, or an MLP in place of attention) becomes less critical and can be selected based on design priorities. Applying attention only to the top- k relevant tokens operates at $\mathcal{O}(N + k^2)$ complexity, where $k \ll N$ and $k \leq \sqrt{N}$, resulting in near-linear scaling with respect to the number of tokens N . Replacing attention with a simple MLP applied to the modulated V yields strictly $\mathcal{O}(N)$ complexity.

We evaluate Co⁴ on ImageNet-1K, Mini-ImageNet, Tiny-ImageNet, CIFAR-10, and reinforcement learning (RL) benchmarks. Across tasks, Co⁴ achieves significantly faster learning with reduced computational demand than a standard Transformer model under the same conditions.

2. Background

The flexible integration of top-down contextual signals (C) and bottom-up sensory evidence (R) provides a cellular substrate for several computational theories of neocortical function (Aru et al., 2020; Bachmann et al., 2020; Marvan et al., 2021; Aru et al., 2021). One prominent framework for such dual-stream processing is predictive coding and related formulations grounded in the principle of free-energy minimization (Friston, 2010; 2005; Friston et al., 2018; 2017). In predictive coding models, predictions (C) generated at higher cortical levels are compared with incoming sensory signals (R), such that inputs consistent with the predictions are attenuated while mismatches propagate upward as prediction errors. However, accumulating evidence (Marvan & Phillips, 2024) suggests that R - C interactions are not limited to purely subtractive comparison. Instead, convergent inputs can interact nonlinearly, such that coherent contextual and sensory signals cooperatively amplify neuronal responses through bursting. Work on burst-dependent synaptic plasticity (Payeur et al., 2021) further indicates that these dendritic R - C interactions support coordinated credit assignment across hierarchical circuits, providing a biologically plausible approximation to gradient-based optimization. However, although such approaches are inspired by TPN mechanisms for learning, their processing dynamics do not directly reflect TPN computation. More broadly, flexible R - C coupling has been linked to integrative processes associated with conscious processing (Aru et al., 2021; Storm et al., 2024; Marvan et al., 2021) and to FF processing across distinct mental-state regimes (Phillips et al., 2024; Graham et al., 2025). These findings motivate the MOD dynamics employed in Co⁴. See A.3 for extended background.

3. Co⁴ Architecture

The Co⁴ mechanism (Figure 1(b)) dynamically tunes latent Q , which acts as evidence (R) (i.e., *what should be looked for*), using contextual input (C) from the evolving K and V . Similarly, latent K , acting as R , evolves in response to the current Q (i.e., *what is being asked*) and the associated values V , which together provide contextual input (C). In turn, V , acting as R , adapts through interaction with the updated Q and K , which together form its contextual input (C). In effect, each internally generated token implicitly evaluates:

“How should I represent myself given what this latent is attempting to understand?”

This reciprocally adaptive loop is implemented through the cooperation of Q-, K-, and V-TPN-inspired populations. In this process, Q-TPNs generate modulated queries Q_m by using latent queries Q_L as R , and input projections Q_X and

K_X , together with the internal belief state μ , as C . Here, Q_X serves as proximal context (P), K_X as distal context (D), and μ as universal context (U), representing a local joint prediction error between evolving latent representations and sensory evidence. The contextual field C is therefore not monolithic but consists of multiple sources that collectively modulate the evidence stream R , analogous to the integration of diverse contextual inputs across dendritic compartments in pyramidal neurons (Adeel et al., 2023a; Pagkalos et al., 2023). This formulation allows Q_m to dynamically align with both sensory evidence and emerging internal hypotheses.

Similarly, K-TPNs generate modulated keys K_m by using latent keys K_L as R , and input projections Q_X and K_X , together with μ , as C . In this configuration, K_X serves as P, Q_X as D, and μ as U. Accordingly, K_m is refined in coordination with evolving internal and sensory signals.

V-TPNs generate modulated values V_m by using latent values V_L as R , and input projection V_X , together with Q_m , K_m , and μ , as C . Here, V_X serves as P, Q_m and K_m as D, and μ as U. Accordingly, V_m evolves through interaction with the jointly updated Q_m and K_m , encoding coherent hypotheses grounded in both internal inference and sensory validation.

For each raw latent token (Q_L, K_L, V_L), Co^4 generates distinct sets of (Q_m, K_m, V_m), each undergoing customized triadic interaction. The resulting coherent Q–K–V representations are then pooled for top- k token attention, or alternatively, only V_m is passed to an MLP layer.

The formal equations below describe the case in which Q_L, K_L , and V_L are initialized from normal distributions. In this setting, strong contextual inputs from the input projections place the system in the AD regime.

The update rule for the internal joint belief state μ , which governs prediction success maximization (Marvan & Phillips, 2024) in Eqs. (7–9) and can be interpreted as a precision-like contextual gain signal in predictive-coding terms, is given by:

$$\mu \leftarrow \mu \odot (1 + \alpha E), \quad (1)$$

where α is the step size, \odot denotes elementwise multiplication, and E represents the aggregated local prediction error that compare latent predictions with modulated representation to update belief state:

$$E = |\epsilon_q| + |\epsilon_k| + |\epsilon_v|, \quad (2)$$

with individual prediction errors given by:

$$\epsilon_q = Q_m - Q_L, \quad \epsilon_k = K_m - K_L, \quad \epsilon_v = V_m - V_L \quad (3)$$

The MOD cooperation laws (Eqs. 4–6), together with the computations of Q_m , K_m , and V_m defined in different formulations (Eqs. 7–12), are grounded in burst-probability transfer functions (Eqs. 20–23, see A.4) derived

for TPNs operating in distinct processing regimes (AA, AD, AD+Awake) (Graham et al., 2025), consistent with the dendritic transfer functions reported in (Kay & Phillips, 2020; Kay et al., 2022). In this formulation, bursting probabilities are translated into a continuous amplitude that reflects the degree of coherence between the R and C streams during the FF phase. The resulting MOD functions therefore define a structured cooperation surface over the R – C variables, shaping representational salience and guiding gradient flow along coherent evidence–context trajectories. These functions can be expressed in the following general forms:

$$\text{MOD}_1(R, C_1, C_2) = f_c(C_1) + g(R, C_2) \quad (4)$$

$$\text{MOD}_2(R, C) = f_r(R) + g(R, C) \quad (5)$$

$$\text{MOD}_3(R_1, R_2, C) = f_r(R_1) + f_c(C) + g(R_2, C) \quad (6)$$

where C_1, C_2, R_1, R_2 represent possible combinations of different types of receptive and contextual fields, including proximal, distal, and universal inputs (Adeel, 2020; Adeel et al., 2023a), and may vary depending on the formulation used (e.g., see Eqs. 7–9). Generally, $f_c(C)$ represents the unilateral integrated contextual drive function, $f_r(R)$ denotes the unilateral integrated evidence function, and $g(R, C)$ represents cooperative interaction, modeled here as a bivariate multiplicative function (alternative interaction forms are possible). Larger values of $\text{MOD}(R, C)$ correspond to highly salient latent representations.

Eq. 4 represents the AD regime and captures high bursting under low R and high C inputs. Since this MOD form lacks an independent evidence-driven term $f(R)$, it encodes a context-governed inductive bias: evidence influences cooperation only through a context-controlled gate, corresponding to high MOD activation, linked to imaginative or internally generated cognition. Consequently, a purely evidence-dominant regime, such as AA is not achievable within this formulation.

Eq. 5 represents the AA regime and captures moderate bursting under high R and moderate C inputs. Salience is primarily driven by sensory evidence R , while context C modulates amplification without dominating. This corresponds to moderate activation supporting perception.

Eq. 6 represents the AD + Awake regime and captures maximum bursting under high R and high C inputs. When both R and C are large, the system enters a maximal coherence regime. In this maximal regime, both unilateral drives and their cooperative interaction are active simultaneously. Both evidence and context independently drive amplification. In this regime, both sources can independently initiate bursting, and their interaction further enhances amplification. This MOD activation supports contextually grounded imagination and inference.

The internally generated (predicted) latent queries are defined as follows:

$$Q_m = (Q_X + \mu) + Q_L(K_X + \mu) \quad (7)$$

This is a MOD function of the form shown in Eq. 4, with

$$R = Q_L, C_1 = Q_X + \mu, C_2 = K_X + \mu$$

where C_1 is an additive combination of the proximal and universal contexts, and C_2 is an additive combination of the distal and universal contexts.

Similarly, the modulated keys are given by:

$$K_m = (K_X + \mu) + K_L(Q_X + \mu) \quad (8)$$

This is a MOD function of the form shown in Eq. 4, with

$$R = K_L, C_1 = K_X + \mu, C_2 = Q_X + \mu$$

where C_1 is an additive combination of the proximal and universal contexts, and C_2 is an additive combination of the distal and universal contexts.

The evolution of latent value tokens is given by:

$$V_m = V_X^2 + 2V_X + (Q_m + \mu)(K_m + \mu)(1 + |V_L|) \quad (9)$$

This asynchronous MOD function follows a form similar to that proposed in (Adeel et al., 2023a)³ but here context drives the interaction due to randomly initialized latents; the specific formulation shown in Eq. 4, with

$$R = 1 + |V_L|, C_1 = V_X^2 + 2V_X, C_2 = (Q_m + \mu)(K_m + \mu)$$

where C_1 is a quadratic function of the proximal context, and C_2 is a composite function of the distal contexts (Q_m, K_m) and the universal context μ . In these MOD functions, when C (i.e., C_1 and C_2) ≈ 0 , evidence R has no influence on cooperation. When both R and C have minimal strengths, they cooperate weakly, a regime termed Apical Cooperation (AC) (Graham et al., 2025). When $|C|$ is moderate to large and $|R|$ is small, cooperation is dominated by contextual self-drive, yielding context-led salience generation consistent with belief-driven or internally generated interpretations, i.e., the AD regime. Overall, in this MOD form, C determines whether R is amplified or attenuated. Figure 1(c) illustrates a general form of the MOD function for the case of a single C and R .

When latents are not initialized from a normal distribution but instead are set via input projections such that $Q_L = Q_X$, $K_L = K_X$, $V_L = V_X$, the resulting Q_m , K_m , and V_m take the following forms:

³The functional form was originally identified empirically in prior audio-visual speech enhancement experiments, where visual context (C) modulated and could dominate noisy auditory evidence (R) under low signal-to-noise ratios. The resulting interaction structure captures context–evidence cooperation and is consistent with the nonlinear transfer functions reported in biophysical models of pyramidal neurons (Graham et al., 2025).

$$Q_m = Q_L + Q_L K_X \quad (10)$$

This is a MOD function of the form shown in Eq. 5, with

$$R = Q_L, C = K_X$$

$$K_m = K_L + K_L Q_X \quad (11)$$

This is a MOD function of the form shown in Eq. 5, with

$$R = K_L, C = Q_X$$

In this formulation, Q_m and K_m operate in AA regime in which activation is determined by R but with modulation by C .

$$V_m = \text{ReLU}_\alpha(V_L^2 + 2V_L + Q_m K_m (1 + |V_L|)) \quad (12)$$

This is a MOD function of the form shown in Eq. 6, with

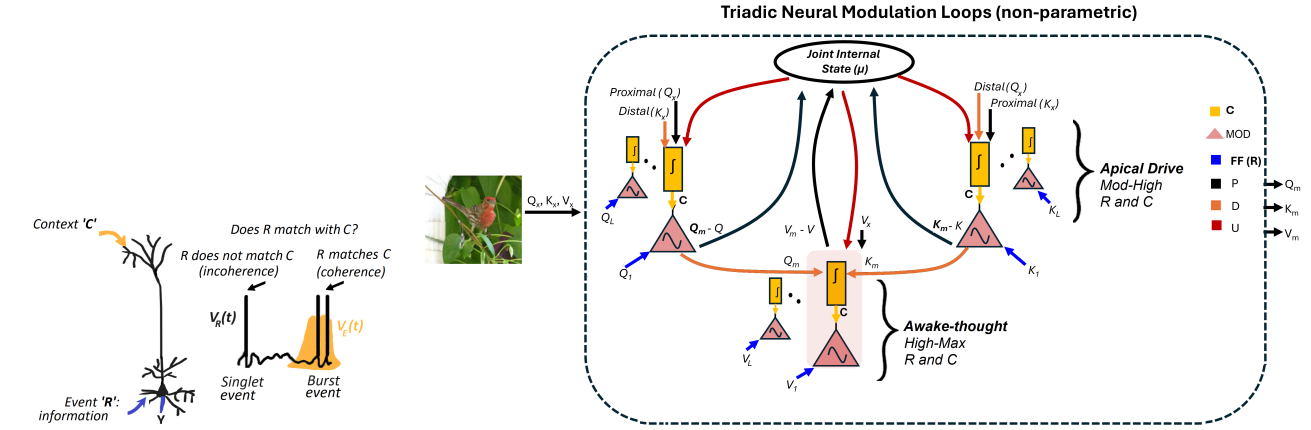
$$R_1 = V_L^2 + 2V_L, R_2 = 1 + |V_L|, C = Q_m K_m$$

The $\text{ReLU}_\alpha(x)$ function is a variant of the Rectified Linear Unit (ReLU) activation function commonly used in deep learning models and is defined as:

$$\text{ReLU}_\alpha(x) = \min(\max(0, x), \alpha)$$

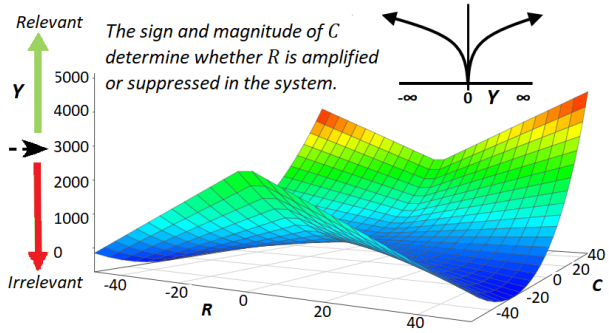
where $\alpha > 0$ is the configurable maximum activation value, $\alpha = 6$ is used in the experiments reported here.

In EQ. 12, C as a ‘modulatory force’ pushes the information to the positive side of the activation function (e.g., ReLU6) if R is relevant, otherwise to the negative side. In essence, strong C can discourage or encourage amplification of neural activity regardless of R ’s strength (strong or weak). The value of C captures the strength of the signal, but different approximate ranges of this value are distinctly associated with different mental-state-dependent processing regimes. The differing behaviour reflects the nonlinearity in the interaction between C and R . Eq. 12, visualized in Figure 1(d) as the general form of the MOD function for the case of a single C and R , includes: an independent evidence term $f(R) = R^2 + 2R$ and an interaction term $g(R, C) = C(1 + |R|)$. This enables nuanced behavior across regimes: when both $R \approx 0$ and $C \approx 0$, cooperation is minimal. When R dominates and C is weak, the evidence term $f(R)$ controls the salience amplitude and gradients. This reflects an AA-like regime, where perception is driven by strong sensory evidence with weak contextual bias.

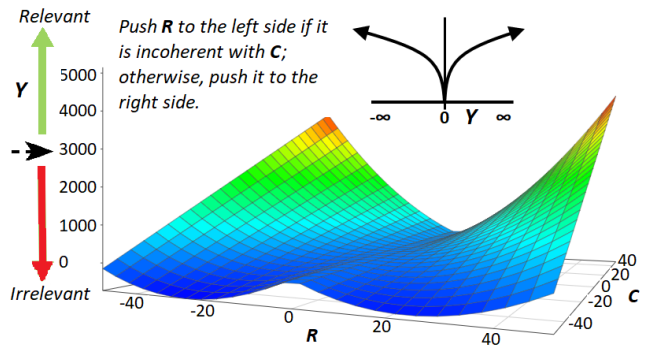


(a) A pyramidal two-point neuron (Larkum et al., 1999; Phillips et al., 2024) integrates receptive field (R) input at the basal dendrites and contextual field (C) input at the apical dendrites. The contextual field includes inputs from diverse sources, including feedback. Their coactivation induces burst firing and selective amplification of coherent signals.

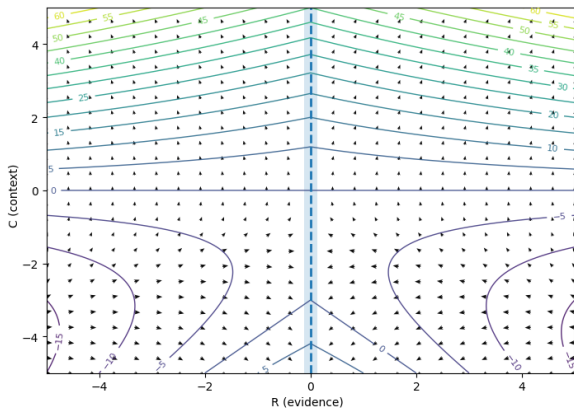
(b) Co^4 architecture: latent Q_L , K_L , and V_L tokens are initialized from a random distribution and serve as feedforward (FF) inputs i.e., receptive fields (R). Contextual input, including Q_X , K_X , and V_X are FF contextual projections that assume proximal (P) or distal (D) roles relative to the active TPN population, whereas μ functions as universal (U) context and provides the recurrent feedback within the iterative dynamics. The TPN-like circuits governing Q_m , K_m , and V_m evolve via MOD dynamics determined by the relative magnitudes of R and C inputs, corresponding to the neurobiological apical drive (AD) and AD + awake processing regimes. The resulting modulated representations Q_m , K_m , and V_m are subsequently selected and passed to the self-attention block, or alternatively, V_m is simply passed to an MLP layer. See A.5 for the basic architecture.



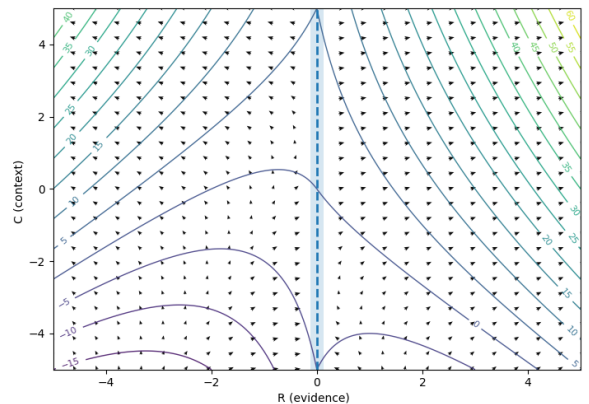
(c) MOD function: $MOD(R, C) = C^2 + 2C + C(1 + |R|)$



(d) MOD function: $MOD(R, C) = R^2 + 2R + C(1 + |R|)$



(e) Vector field visualization and contour plots: $MOD(R, C) = C^2 + 2C + C(1 + |R|)$



(f) Vector field visualization and contour plots: $MOD(R, C) = R^2 + 2R + C(1 + |R|)$

Figure 1. Integrated view of biologically inspired mechanisms: (a) Pyramidal two-point neuron; (b) Co^4 triadic reasoning via Q - K - V interactions; (c-d) MOD function dynamics illustrating context-sensitive filtering; Y represents the FF signal, which is separated into relevant and irrelevant streams depending on the strength of C ; (e-f) MOD contours and vector fields across the R - C space. Surface plots are presented over a wider range of R and C to illustrate the global geometry of the cooperation landscape, while contour and vector-field visualizations focus on a smaller range to highlight local gradient flow and regime transitions near the origin. Variations in the strengths of R and C shift the system across distinct processing regimes analogous to the neurobiological AA, AD, and AD+Awake regimes, producing corresponding geometric deformations in gradient flow. By shaping representations prior to downstream readout, these modulation laws guide optimization along R - C interaction manifolds, reducing propagation through noisy or irrelevant directions.

When both R and C are strong, the system achieves large amplitude and well-directed gradients. This corresponds to the AD + Awake regime of grounded imagination, where context actively tests and refines evidence for maximal coherence. Eqs. (10-11), by contrast, reflect a simpler, additive cooperation model. This supports a perception-like AA regime, where context modulates but does not dominate evidence. See A.7 for spiking simulations of context-sensitive pyramidal neurons implementing interaction dynamics similar to Eq. 12, where bursting probabilities across varying strengths of R and C exhibit regime transitions.

The specific form of the triadic modulation loops and the R - C integration strategies may vary across datasets and hyperparameter configurations. For example, Figure 1(b) represents one of the architectural variants evaluated in this paper, building on the basic architecture (see A.5); other architectural instantiations are possible. The key element, however, is the cooperative modulation dynamics ($\text{MOD}(R, C)$) operating under distinct mental-state-dependent processing regimes (Phillips et al., 2024; Graham et al., 2025).

3.1. Gradient Flow

Rather than assigning global credit exclusively during the feedback (FB) phase via standard backpropagation to reduce prediction error, Co^4 introduces local, credit-like contextual signals from neighboring neurons during the FF phase. These signals, together with joint local prediction error represented by the internal state μ , allow representations to be adaptively refined on the fly prior to global supervision. This constitutes an unsupervised representational shaping phase that precedes task-driven weight updates. Global FB through standard backpropagation is then used to fine-tune connection weights with respect to the task objective. This hybrid local-global mechanism facilitates the rapid emergence of relevant features at early stages, contributing to faster learning.

Co^4 achieves gradient stability by shaping the underlying R - C response surface through triadic modulation prior to the downstream readout. The MOD function defines a structured cooperation field over receptive and contextual variables, such that representations are never raw but are generated directly within a context-conditioned dynamical phase space. As a result, gradients propagate along coherent trajectories defined by the geometry of the cooperation field rather than through entangled input space.

From a dynamical systems perspective, the vector field (Figure 1(e)) induced by Eq. 9 (the general form of the MOD function) corresponds to the gradient of the cooperation surface, where each vector encodes the local direction and magnitude of maximal semantic amplification. Regions of strong contextual coherence produce smooth, directed flows, enabling stable gradient propagation along cognitively meaningful pathways. Conversely, regions of con-

textual mismatch naturally induce attenuated or saturating dynamics, preventing abrupt transitions and suppressing unstable gradient spikes. However, gradients remain anchored by context, so no learning signal flows through the RF channel when context is off. Hence, learning signals can vanish globally. This cooperation law does not support a genuine AA regime, since evidence cannot drive cooperation or gradients in the absence of contextual input. In Eq. 12, gradients remain anchored by evidence (Figure 1(f), so learning signals rarely vanish globally; both channels can carry gradient. Gradients grow at most linearly in $|R|$ (no exponential blow-up).

Crucially, in the Co^4 formulation, vanishing and exploding gradients reflect distinct mental regimes of the system. These regimes correspond operationally to low-coherence interaction patterns. Stable learning emerges in regimes, where receptive and contextual streams are coherently aligned and gradients flow along well-conditioned semantic manifolds. Because reasoning is embedded within a single layer and mediated by continuous cooperation dynamics, Co^4 reduces reliance on architectural depth for constructing relational structure. This shortens effective gradient paths and ensures that learning is governed primarily by the geometry of R - C coherence rather than by the accumulation of transformations across deep stacks.

Hence, Co^4 stabilises learning not by engineering gates or optimisers, but by reshaping the response surface prior to downstream readout. A possible extension of the current formulation would incorporate global FB (error) signals directly into processing via online learning rules, such as burst-dependent synaptic plasticity (Payeur et al., 2021; Greedy, 2022), thereby further integrating local and global credit signals simultaneously.

4. Results

ViT⁴ (Dosovitskiy, 2020) is used as the baseline for comparison against Co^4 . Figures 2 and 3 visually demonstrate how Co^4 selects relevant information before paying attention. Detailed analysis proceeds as follows: For classification tasks on ImageNet-1K, Mini-ImageNet, Tiny-ImageNet, and CIFAR-10, Co^4 with latent initialization from a normal distribution (Eqs. 7-9) is directly compared against the standard Transformer baseline (Dosovitskiy, 2020). For classification on Mini-ImageNet, Co^4 with an MLP (no attention) and latent initialization from input projection (Eqs. 10-12) is evaluated. For reinforcement learning (RL) tasks, Co^4 with latent initialization from input projection (Eqs. 10-12) is benchmarked against the architecture proposed in (Tang & Ha, 2021).

Across experiments, Co^4 consistently achieves superior val-

⁴https://github.com/google-research/vision_transformer?tab=readme-ov-file

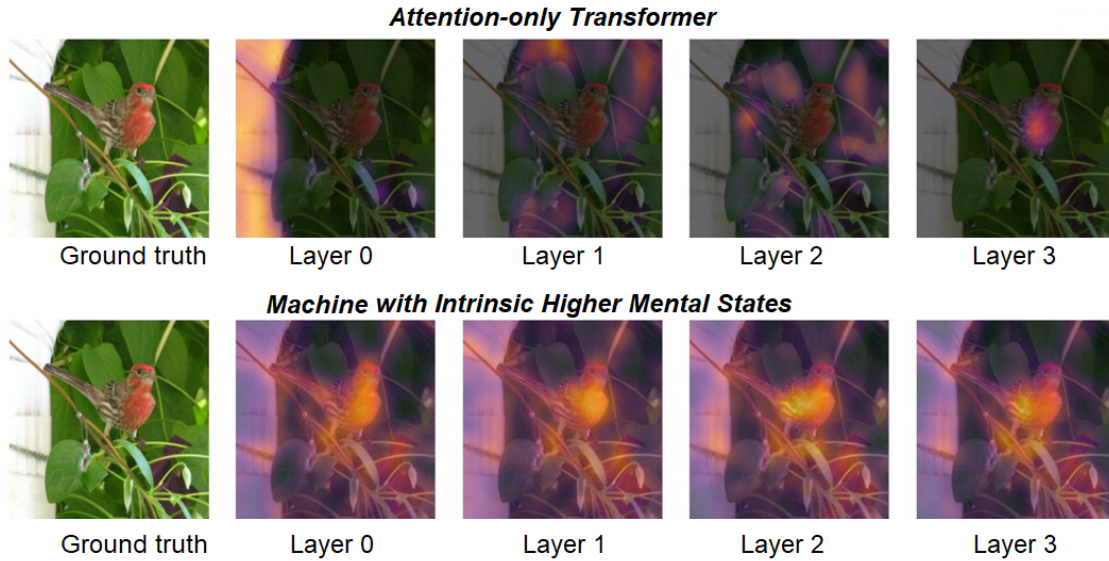


Figure 2. Early training comparison between an attention-only Vision Transformer (ViT) (Dosovitskiy, 2020), trained from scratch, and a Co^4 machine endowed with intrinsic mental-state-dependent processing regimes analogous to awake imaginative processing (Phillips et al., 2024; Graham et al., 2025), which pre-select relevant information *before* attention is applied. The task is to identify a bird from the Mini-ImageNet dataset. Brightness indicates regions emphasized. In the ViT model, this is after attention. In contrast, Co^4 rapidly forms a coherent interpretation of the input, highlighting the top- k salient regions via internally generated awake imaginative regimes *before* attention is computed. Co^4 exhibits earlier and sharper activation over the semantically relevant object (bird), indicating more coherent internal inference. These findings raise questions about the necessity of deep attention stacks.

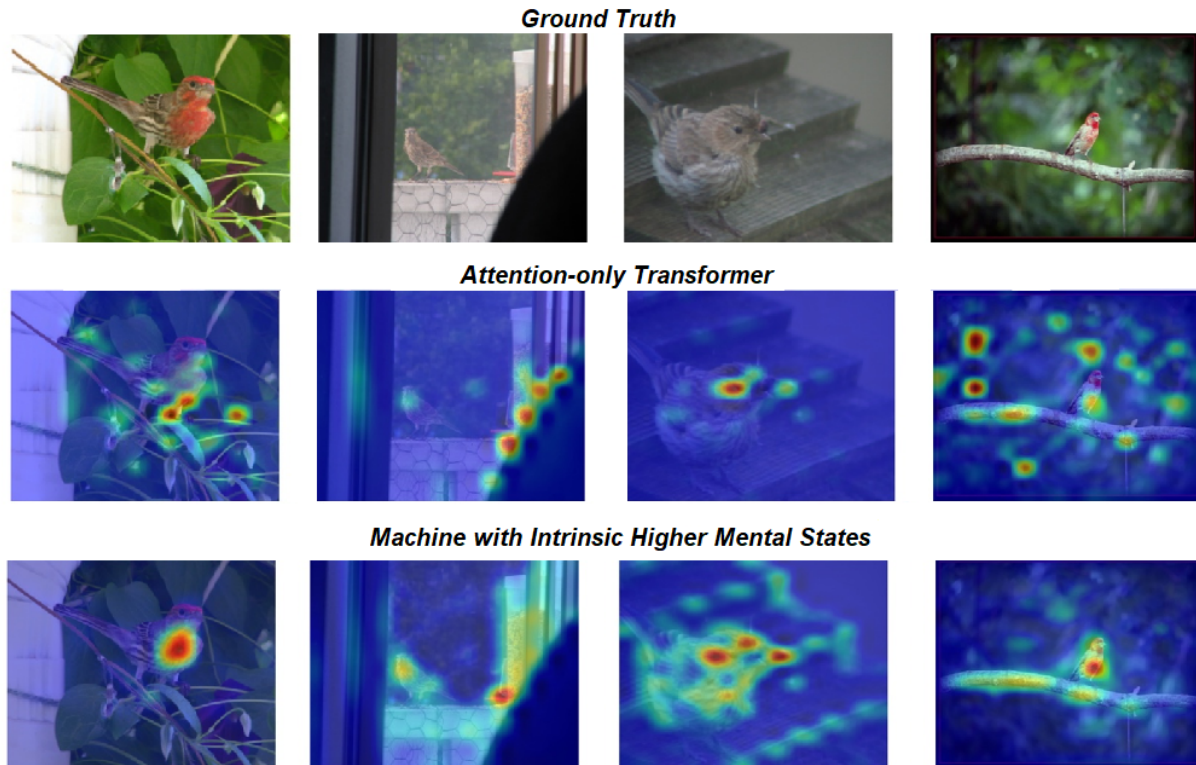


Figure 3. The figure visualizes the complete attention distribution over N input tokens: a single-layer Co^4 machine versus an attention-only ViT (Dosovitskiy, 2020), both trained on Mini-ImageNet for 30 epochs. The ViT exhibits more dispersed attention with less selective localization. In contrast, Co^4 demonstrates more centered, context-sensitive activation patterns, indicating stronger spatial coherence.

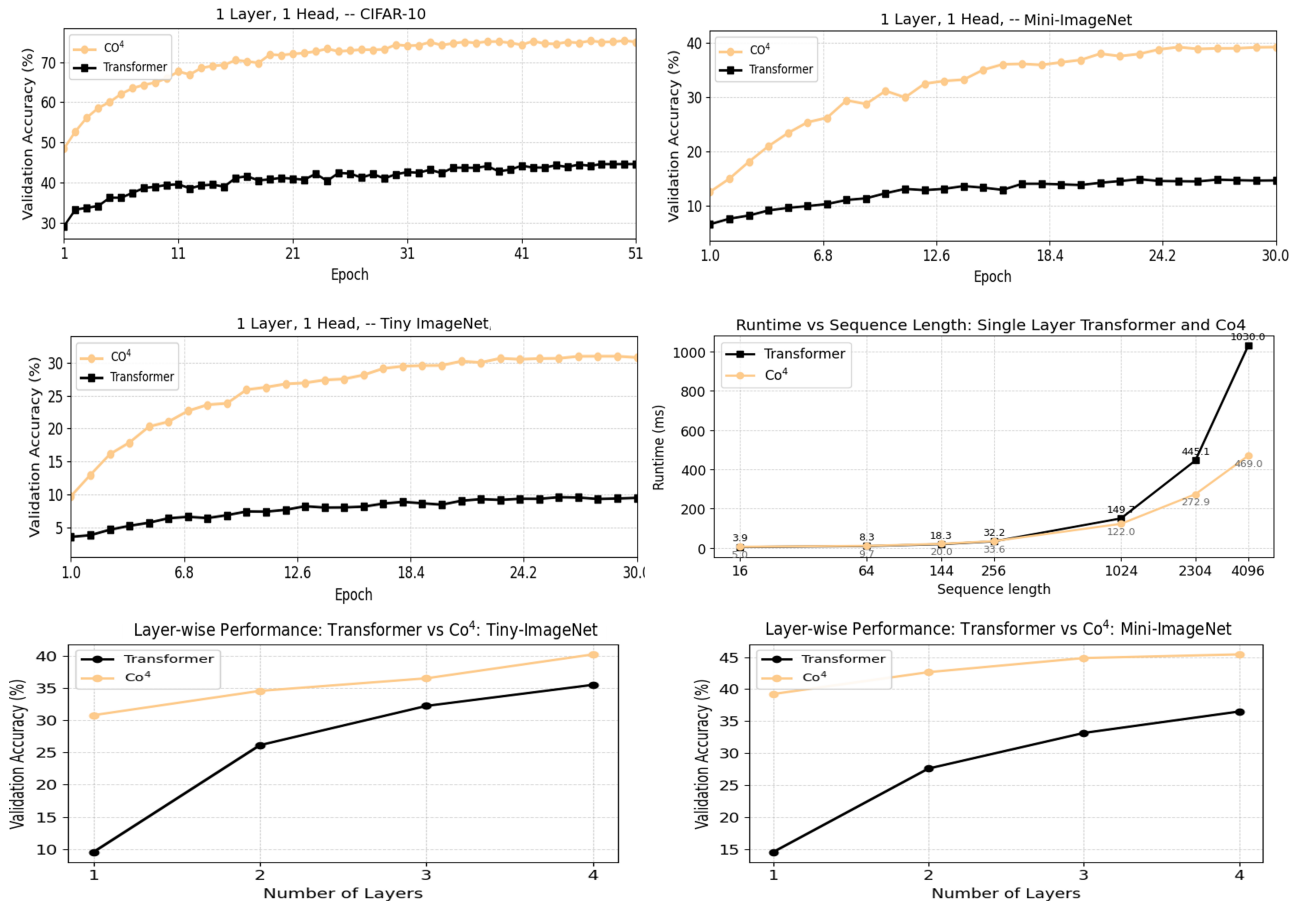


Figure 4. Co⁴ versus Transformer on CIFAR-10, Tiny-ImageNet, and Mini-ImageNet, trained from scratch: (i–iii) performance of a single-layer model; (iv) inference runtime as a function of sequence length for a single layer (see A.6 for theoretical computational cost analysis); and (v–vi) layer-wise validation accuracy on Tiny-ImageNet and Mini-ImageNet.

validation accuracy with significantly fewer layers and attention heads, and converges more rapidly than the standard Transformer using either top-*k* or simple MLP downstream (no attention) readouts, with computational complexities of $\mathcal{O}(N + k^2)$ and strictly $\mathcal{O}(N)$, respectively. In contrast, the baseline Transformer typically requires deeper stacks, more attention heads, and longer training schedules to reach comparable performance. This performance gap arises because Co⁴ embeds coherence constraints directly into the representation formation process, allowing the model to identify relevant structures before any downstream readout is applied. Standard attention mechanisms, by contrast, approximate these dynamics only after substantial architectural depth and contextual accumulation.

We also observed that single-step Co⁴ modulation (without μ) achieves performance comparable to its iterative version (with internal belief state μ). In tested environments, a single inference pass appears sufficient to reach a stable representational fixed point. However, in some cases, the iterative Co⁴ loop, with predictive refinement through an

internal state U , converged slightly faster to ceiling accuracy. This suggests that coherence can often be established in one step, with marginal gains from further iterations on classification tasks. Additional Co⁴ iterations may be more beneficial in settings with increased noise, partial observability, or temporally evolving inputs. All results reported below correspond to the single-step modulation setting.

4.1. Image Classification: ImageNet-1K, Mini-ImageNet, Tiny-ImageNet, CIFAR-10

Figure 4 and Table 1 present a comparative analysis between ViT and Co⁴ under same training setup. Despite operating at a lower computational complexity of $\mathcal{O}(12^2)$, where $k = 12$ remained constant across all experiments, the Co⁴ model significantly outperforms the ViT, which incurs a higher complexity of $\mathcal{O}(196^2)$, in terms of learning speed and convergence on the Mini-ImageNet, Tiny-ImageNet, and CIFAR-10 datasets for $N = 196$. Moreover, Co⁴ with a simple MLP downstream module (without attention) performs better than Co⁴ with top-*k* attention (Table 1).

Table 1. Comparison between Transformer and Co⁴ models across ImageNet-1K, Mini-ImageNet, Tiny-ImageNet, and CIFAR-10: L, H, Params, and Acc denote the number of layers, attention heads, model parameters, and accuracy, respectively.

Dataset	Model	L	Combination	Hidden	MLP	H	Params.	Acc.
ImageNet-1K	Co ⁴	8	Co ⁴	768	3076	1	53.4M	70.24%
	Co ⁴	6	Co ⁴	768	3076	1	40.4M	67.30%
	Co ⁴	6	4 Co ⁴ + 2 MHSA	768	3076	1	41.6M	75.01%
	Transformer	12	MHSA	768	3076	12	86M	74.80%
Mini-ImageNet	Co ⁴	1	Co ⁴	384	3076	1	2.0M	39.20%
	Co ⁴	4	Co ⁴	384	3076	1	8M	45.40%
	Co ⁴ -MLP	1	Co ⁴	384	3076	1	1.87M	40.21%
	Co ⁴ -MLP	4	Co ⁴	384	3076	1	6.07M	48.92%
	Transformer	1	MHSA	384	3076	1	2.2M	14.60%
	Transformer	4	MHSA	384	3076	1	8.8M	36.80%
Tiny-ImageNet	Co ⁴	1	Co ⁴	384	3076	1	1.8M	30.90%
	Co ⁴	4	Co ⁴	384	3076	1	7.2M	40.20%
	Transformer	1	MHSA	384	3076	1	1.9M	9.50%
	Transformer	4	MHSA	384	3076	1	7.6M	35.60%
CIFAR-10	Co ⁴	1	Co ⁴	384	3076	1	1.6M	75.20%
	Co ⁴	4	Co ⁴	384	3076	1	6.4M	80.30%
	Transformer	1	MHSA	384	3076	1	1.8M	44.60%
	Transformer	4	MHSA	384	3076	1	7.2M	80.20%

Table 2. Effect of varying the number of attention heads on Co⁴ performance: L, H, Ep, and Acc denote the number of layers, attention heads, epochs, and accuracy, respectively.

Dataset	L	H	Ep.	Embedding	Acc.
Imagenet-1k	6	1	300	768	67.30%
	6	6	300	768	67.81%
	6	12	300	768	67.89%
Cifar10	4	1	30	384	80.30%
	4	4	30	384	80.36%

On large-scale ImageNet-1K, only the top-*k* variant is evaluated and reported here. An eight-layer Co⁴ model achieves 70.24% top-1 accuracy with 53.4M parameters. Notably, a hybrid configuration with four Co⁴ layers interleaved with two standard multi-headed self attention (MHSA) layers achieves 75.01%, compared to a twelve-layer Transformer (74.80%) while using less than half the parameters (41.6M vs. 86M). Testing of Co⁴ with a simple MLP downstream module (without attention) on ImageNet-1K, and comparisons with newer variants such as Swin-T (Liu et al., 2021), DeiT-S (Touvron et al., 2021), and VMamba-T (Liu et al., 2024), remain part of ongoing work.

Inference runtime (Figure 4, row 2, column 2) While both models exhibit comparable inference times at short sequence lengths, where the quadratic cost of attention has not yet become dominant, their runtimes diverge as sequence length increases. Specifically, the Transformer’s inference time grows rapidly, exhibiting the expected quadratic scaling. In contrast, Co⁴ demonstrates significantly slower growth,

approximating linear scaling. This empirically supports the core claim of Co⁴: by circumventing the quadratic bottleneck of attention, it enables substantially greater scalability for long-context reasoning. A detailed derivation is provided in A.6.

Layer-wise comparison (Figure 4, last row): Compares the layer-wise validation accuracy of a standard attention-only Transformer and the Co⁴ model with top-*k* on Tiny-ImageNet and Mini-ImageNet. Across both datasets, Co⁴ consistently outperforms the Transformer at all depths. Notably, Co⁴ achieves strong performance even with a single layer, whereas the Transformer exhibits very poor accuracy in the shallow regime and requires additional depth to approach comparable performance. These results indicate that Co⁴ establishes coherent internal representations with significantly fewer layers than standard Transformers, supporting the claim that intrinsic mental-state-dependent processing regimes enable depth-efficient learning by pre-selecting and amplifying relevant information before attention is applied.

Effect of number of heads (Table 2): Varying the number of attention heads in Co⁴ results in only marginal performance differences across datasets. On ImageNet-1k, increasing the number of heads from 1 to 12 yields an absolute improvement of less than 1%. This indicates that multi-head attention is not a critical factor for performance in the Co⁴ architecture. This behavior can be attributed to the token modulation and aggregation/generation mechanisms, which enforce strong feature interactions and selective information routing prior to attention. It implies that token modulation may already perform a role analogous to multi-head mixing.

Table 3. Effect of different modulation equations on CIFAR-10 performance (4 layers, 1 head, 30 epochs, 384-dimensional embeddings).

Modulation Equations	Acc.
$Q_m = Q_X + Q_L \cdot K_X$ $K_m = K_X + K_L \cdot Q_X$ $V_m = V_X^2 + 2V_X + Q_m K_m (1 + V_L)$	78%
$Q_m = Q_L + Q_L \cdot Q_X$ $K_m = K_L + K_L \cdot K_X$ $V_m = V_X^2 + 2V_X + Q_m K_m (1 + V_L)$	69%
$Q_m = Q_L + Q_L \cdot K_X$ $K_m = K_L + K_L \cdot Q_X$ $V_m = V_X^2 + 2V_X + Q_m K_m (1 + V_L)$	72%
$Q_m = Q_X + Q_L \cdot K_X$ $K_m = K_X + K_L \cdot Q_X$ $V_m = V$	68%
$Q_m = Q_X + Q_L \cdot K_X$ $K_m = K_X + K_L \cdot Q_X$ $V_m = V_X + V_L \cdot Q_m \cdot K_m$	68%

This suggests that the proposed architecture is robust to the choice of head count in the tested regimes, allowing a single head to achieve comparable performance with reduced computational overhead.

Regime-collapse ablation studies (Table 3): This regime-collapse ablation studies show that cooperation laws inspired by mental-state-dependent processing regimes are not arbitrary. Modifying their functional form or nonlinear structure degrades performance, suggesting that preserving the qualitative structure of the MOD formulation is important for achieving optimal results. This provides empirical support for the biological mapping.

Top- k token selection and bottleneck effects (Table 4): Reducing the number of generated tokens via top- k feature leads to improved performance in Co⁴ whereas the same top- k feature approach in ViT reduces the performance. This sharply contrasts with the typical behavior of Transformer-based models, which often benefit from increased context length. In Co⁴, however, the opposite trend emerges: *less information leads to better performance*. This provides direct empirical evidence that selective perception can outperform exhaustive perception, supporting the principle that effective reasoning requires internal filtering and compression rather than maximal context exposure.

Table 4. Top- k token selection study comparing Co⁴ with Transformer (ViT) under identical architectural settings. Performance is shown for multiple values of k , together with the ViT baseline (Dosovitskiy, 2020): L, Tok, k , Acc, and BL denote the number of layers, total tokens, the top- k threshold, top- k accuracy, and baseline ViT accuracy, respectively.

Dataset	Model	L	Tok.	k	Acc.	BL
Tiny-ImageNet	Co ⁴	4	64	44	31%	–
	Co ⁴	4	64	32	33%	–
	Co ⁴	4	64	8	40%	–
	Co ⁴	4	64	3	37%	–
	ViT	4	64	8	32%	35%
	Co ⁴	4	64	8	40%	–
	ViT	1	64	8	6%	9%
	Co ⁴	1	64	8	35%	–
	Mini-ImageNet	Co ⁴	4	256	128	40%
Co ⁴		4	256	64	42%	–
Co ⁴		4	256	32	43%	–
Co ⁴		4	256	16	45%	–
ViT		4	256	16	33%	37%
ViT		1	256	16	12%	14%
Co ⁴		4	256	16	45%	–
Co ⁴		1	256	16	16%	–
CIFAR-10		ViT	4	64	6	76%
	Co ⁴	4	64	6	80%	–

4.2. Reinforcement Learning

In the multisensory RL, V and K are functions of the Sensors 1-N i.e., input $x \in \mathbb{R}^N$ (e.g., any linear or non-linear transformations) and Q is the output of latent positional encoding. For permutation invariance (PI), the latent Q is independent of the input x so that permutation x only affects K and V but not Q , which allows the output to be PI (Tang & Ha, 2021). As explained comprehensively in (Tang & Ha, 2021), the individual sensory inputs 1-N or observations $O_t^i, i=1, 2, \dots, N$ along with the previous action a_{t-1} passes through a neural net (NN) module in an arbitrary order such that each NN has partial access to agent’s observation at time t and i^{th} neuron can only see the i^{th} component of the observation $O_t[i]$, computing $f_K(O_t[i], a_{t-1})$ and $f_V(O_t[i])$ explained in (Tang & Ha, 2021). The overall operation can be described using Eqs. (13-15):

$$K(O_t, a_{t-1}) = \begin{bmatrix} f_K(O_t[1], a_{t-1}) \\ \dots \\ f_K(O_t[N], a_{t-1}) \end{bmatrix} \in \mathbb{R}^{N \times d_{f_K}} \quad (13)$$

$$V(O_t) = \begin{bmatrix} f_V(O_t[1]) \\ \dots \\ f_V(O_t[N]) \end{bmatrix} \in \mathbb{R}^{N \times d_{f_V}} \quad (14)$$

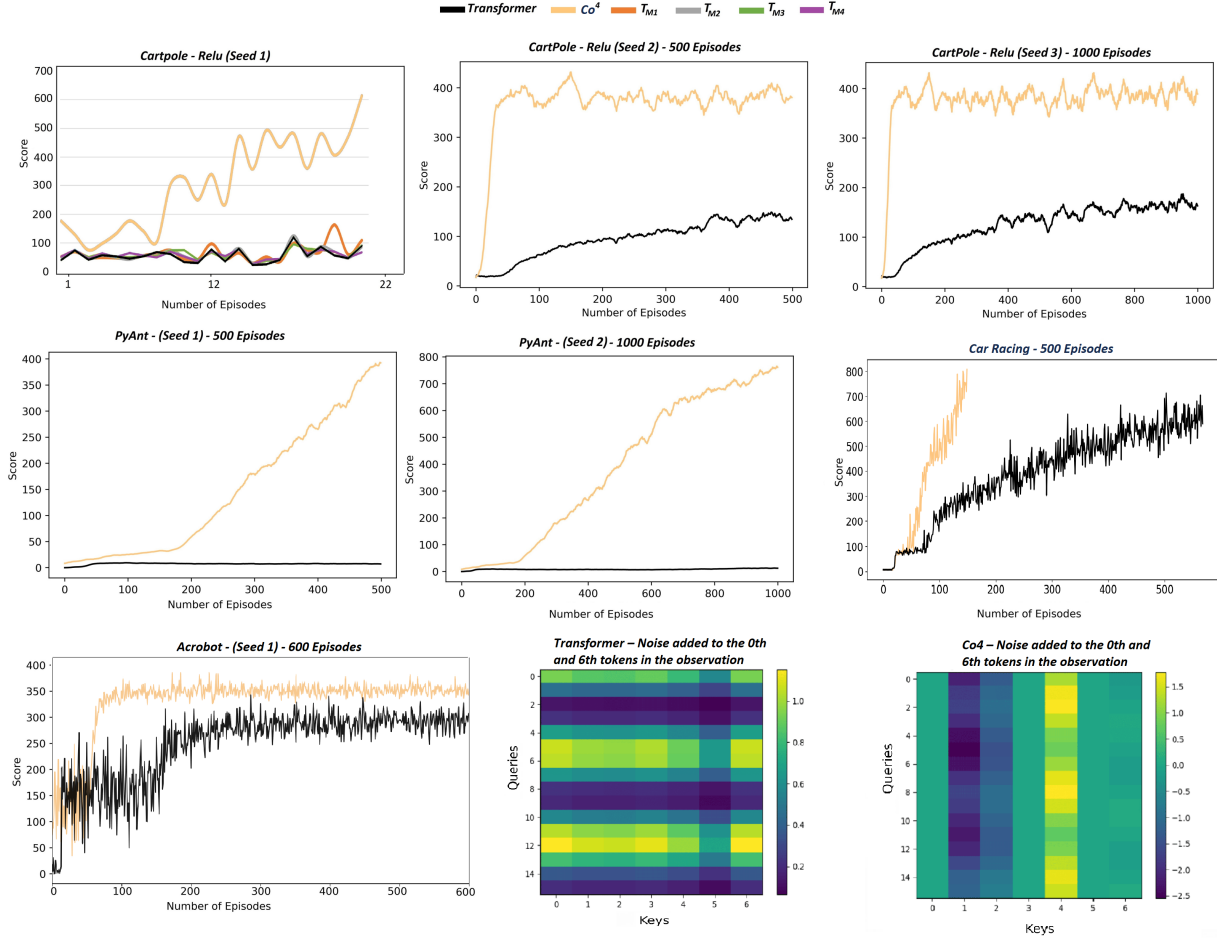


Figure 5. Training results across CartPole (i–iii), PyBullet Ant (iv–v), CarRacing (visual input: $96 \times 96 \times 4$) (vi), and Acrobot (vii), with heat maps (viii–ix) provided as empirical evidence. T_{M1} – T_{M4} denote alternative well-established TPN-inspired asynchronous MOD functions (Kay & Phillips, 2020) (see A.3).

$$m_t = \text{ReLU6}(R(O_t, a_{t-1})^2 + 2R(O_t, a_{t-1}) + C(1 + |R(O_t, a_{t-1})|)) \quad (15)$$

The architectures of the policy networks, training methods, attention neuron layers, and hyperparameters in all agents are the same as used in (Tang & Ha, 2021). The results presented in Figure 5 were generated using the code provided in (Tang & Ha, 2021), which also serves as the baseline.

It was observed that the Co^4 -driven agent learned tasks significantly faster than the state-of-the-art Transformer-based RL agents (Tang & Ha, 2021). Additionally, the previously proposed context-sensitive neuromodulation transfer functions (Eqs. 16–19 in A.3) performed comparably to the Transformer baseline on the CartPole RL task.

Across different random seeds in the CartPole task, Co^4 consistently converged to the maximum fitness score in fewer episodes compared to the Transformer baseline. Similar trends were observed in the PyBullet Ant task, the CarRacing task, which uses a high-dimensional visual input space of $96 \times 96 \times 4$, and the Acrobot task (Järnil Pérez, 2024).

Testing results for CartPole (Table 5) show that Co^4 , trained over 1K–10K episodes, achieved significantly higher fitness scores with much lower standard deviation in both shuffled and unshuffled settings. While Co^4 and the baseline performed comparably in the shuffled 1K-episode setting, Co^4 quickly surpassed the baseline by 5K episodes, maintaining high performance with reduced variance.

In the PyBullet Ant task (Table 6), Co^4 consistently outperformed the baseline across both shuffled and unshuffled scenarios. Similar patterns were also observed in the Acrobot-v1 (Table 7) and MountainCarContinuous (Järnil Pérez, 2024) (Table 8) tasks. Finally, to provide explainability and empirical insight, attention heatmaps for CartPole visualize the attention scores for both the Transformer and Co^4 models under noisy input conditions:

$$[\text{Noise}, x, \dot{x}, \cos(\theta), \sin(\theta), \dot{\theta}, \text{Noise}].$$

Here, keys and values are generated from the observations, while queries are generated independently. The objective is to identify which observation variables are most relevant for

Table 5. CartPole test scores for 1K to 10K episodes.

Model	1K	5K	10K
Transformer	279	340	340
Trans. (Shuffled)	279	339	340
Co ⁴	428	524	538
Co ⁴ (Shuffled)	267	508	536

Table 7. Acrobot test scores after 200 and 400 training episodes.

Model	200	400
Transformer	243	274
Co ⁴	344	350

maximizing cumulative reward. After 100 training episodes: The Transformer assigns substantial attention to the injected noise dimensions. The Co⁴ model effectively suppresses noise, assigning near-zero attention to irrelevant inputs and focusing on the physically meaningful variables.

4.3. Empirical Comparison of Regime-Dependent MOD Formulations

Empirically, different MOD formulations were most effective for different tasks. In CarRacing (RL), Eqs. (10–11) yielded the best performance. In CartPole, PyAnt, Acrobot, and MountainCar, Eq. 12 outperformed the alternatives. For image classification tasks, when latents were initialized from normal distributions, the nonlinear MOD functions (Eqs. 7–9) performed best. When latents were initialized via input projections in Co⁴ with an MLP (no attention), Eqs. (10–12) yielded superior performance.

These findings suggest that different tasks benefit from different regime-dependent processing dynamics. For example, AA-like regimes appear more suitable for RL tasks where sensory evidence plays a dominant role, whereas AD + Awake-like regimes are more effective when both contextual inference and evidence integration are required. Similarly, in image classification, when latents are initialized from a normal distribution, Eqs. (7–9) corresponding to the AD regime are more suitable, as the latents do not directly represent the input (X), which is instead incorporated through strong contextual signals.

In contrast, when latents are initialized directly from input projections (X), Eqs. (10–12), corresponding to AA and AD + Awake regimes, are more appropriate since both evidence and context provide strong signals. These empirical results indicate that no single MOD formulation is universally optimal. Rather, different regime-dependent dynamics are better suited to different task domains, suggesting that regime-dependent processing provides task-adaptive induc-

Table 6. PyBullet Ant test scores after 1K episodes.

Model	ES	ES (Shuffled)
Transformer	121	30
Co ⁴	1170	280

Table 8. MountainCarContinuous test scores after 50–250 training episodes.

Model	50	100	150	200	250
Transformer	0.58	0.21	0.41	0.21	0.23
Co ⁴	0.69	0.42	0.45	0.48	0.46

tive biases rather than enforcing a fixed operating mode.

Code Availability: The implementation of the multi-layered Co⁴ model and all results are reproducible using the released open-source code, which includes training scripts with hyperparameters, evaluation pipelines, configuration files, and pretrained checkpoints.

5. Limitations and Conclusion

Experiments conducted under constrained computational resources demonstrate that Co⁴ can substantially accelerate learning while reducing computational demands. By embedding context–evidence cooperation directly into representation formation, the architecture enables models to identify relevant information prior to downstream readout, reducing reliance on architectural depth and quadratic attention scaling. While scaling to ImageNet-1K indicates promising potential, the full compound effects of the Co⁴ architecture remain to be systematically evaluated. Preliminary experiments using Co⁴ with a simple MLP as a downstream readout, operating at $\mathcal{O}(N)$ computational cost, indicate the potential for further improvements in both effectiveness and efficiency. Ongoing evaluations on larger datasets aim to clarify these trends and will be reported in future work.

Realizing the full design space of Co⁴ requires rigorous investigation of alternative contextual integration strategies, diverse triadic modulation loop configurations, and joint belief update mechanisms, informed by principles from both modern machine learning and cellular neurobiology. Such exploration is computationally demanding; therefore, we release the framework as an open research platform to facilitate community-driven investigation and iterative refinement of the core mechanism. Whether Co⁴ improves asymptotic scaling behavior at very large compute budgets remains an open question.

The initial evidence presented here suggests that architectures inspired by the cellular foundations of higher mental states may provide a promising path toward deep, deliberate imaginative reasoning in artificial systems. This approach opens the door not only to implementing large numbers of lightweight, inference-efficient AI modules but also to moving these systems beyond mere information processing toward contextual reasoning, shifting from raw efficiency to real understanding. Overall, emulating context–evidence cooperation observed in cortical computation could represent a conceptual step toward more cognitively meaningful machine intelligence.

Impact Statement

Whether such advancements are used for beneficial or harmful purposes will ultimately depend on human choices. We hope that the prosocial capacities that have shaped human societies (Bregman, 2020) will guide their development toward the benefit of society. For broader impact, see A.8.

6. Acknowledgments

Advanced Research + Invention Agency (ARIA): Nature Computes Better Opportunity seeds. Cooperation is All You Need (Adeel et al., 2023b) Team. TREND project team (<https://cmilab.org/aichip/team/>), PhD students and post-docs, including Mohsin Raza, Talha Bin Riaz, Noor Ul Zain, Eamin Ch, Reyhane Ahmadi, Khubaib Ahmed. Professor Bill Phillips, Professor Leslie Smith, and Professor Bruce Graham from the University of Stirling. Dr James Kay from the School of Mathematics, University of Glasgow. Professor Johan Frederik Storm (Professor in Neurophysiology) from the University of Oslo. Professor Panayiota Poirazi from IMBB-FORTH. Professor Newton Howard from Oxford Computational Neuroscience. Professor John Broome (Emeritus White’s Professor of Moral Philosophy) from Corpus Christi College, University of Oxford. Professor Peter König from the University Osnabrück. Professor Heiko Neumann from Ulm University, and several other eminent scholars for their help and support in several different ways, including reviewing this work, appreciation, and encouragement. We also acknowledge ChatGPT for its assistance with proofreading and coding support.

References

- Adeel, A. Conscious multisensory integration: Introducing a universal contextual field in biological and deep artificial neural networks. *Frontiers in Computational Neuroscience*, 14, 05 2020. doi: 10.3389/fncom.2020.00015.
- Adeel, A. Beyond attention: Toward machines with intrinsic higher mental states. *arXiv preprint arXiv:2505.06257*, 2025.
- Adeel, A., Adetomi, A., Ahmed, K., Hussain, A., Arslan, T., and Phillips, W. A. Unlocking the potential of two-point cells for energy-efficient and resilient training of deep nets. *IEEE Transactions on Emerging Topics in Computational Intelligence*, 7(3):818–828, 2023a.
- Adeel, A., Muzaffar, J., Ahmed, K., and Raza, M. Cooperation is all you need. *arXiv preprint arXiv:2305.10449*, 2023b.
- Aru, J., Siclari, F., Phillips, W. A., and Storm, J. F. Apical drive—a cellular mechanism of dreaming? *Neuroscience & Biobehavioral Reviews*, 119:440–455, 2020.
- Aru, J., Suzuki, M., and Larkum, M. Cellular mechanisms of conscious processing. *Trends in Cognitive Sciences*, 25, 10 2021. doi: 10.1016/j.tics.2020.07.006.
- Azevedo, F. A., Carvalho, L. R., Grinberg, L. T., Farfel, J. M., Ferretti, R. E., Leite, R. E., Filho, W. J., Lent, R., and Herculano-Houzel, S. Equal numbers of neuronal and nonneuronal cells make the human brain an isometrically scaled-up primate brain. *Journal of Comparative Neurology*, 513(5):532–541, 2009.
- Bachmann, T., Suzuki, M., and Aru, J. Dendritic integration theory: a thalamo-cortical theory of state and content of consciousness. *Philosophy and the Mind Sciences*, 1(II), 2020.
- Bi, X., Chen, D., Chen, G., Chen, S., Dai, D., Deng, C., Ding, H., Dong, K., Du, Q., Fu, Z., et al. Deepseek llm: Scaling open-source language models with longtermism. *arXiv preprint arXiv:2401.02954*, 2024.
- Blankenburg, W. and Mishara, A. L. First steps toward a psychopathology of “common sense”. *Philosophy, psychiatry, & psychology*, 8(4):303–315, 2001.
- Bono, J. and Clopath, C. Modeling somatic and dendritic spike mediated plasticity at the single neuron and network level. *Nature communications*, 8(1):706, 2017.
- Bregman, R. *Humankind: A hopeful history*. Bloomsbury Publishing, 2020.
- Dosovitskiy, A. An image is worth 16x16 words: Transformers for image recognition at scale. *arXiv preprint arXiv:2010.11929*, 2020.
- Friston, K. A theory of cortical responses. *Philosophical transactions of the Royal Society B: Biological sciences*, 360(1456):815–836, 2005.
- Friston, K. The free-energy principle: a unified brain theory? *Nature reviews neuroscience*, 11(2):127–138, 2010.

- Friston, K. J., Parr, T., and de Vries, B. The graphical brain: Belief propagation and active inference. *Network neuroscience*, 1(4):381–414, 2017.
- Friston, K. J., Rosch, R., Parr, T., Price, C., and Bowman, H. Deep temporal models and active inference. *Neuroscience & Biobehavioral Reviews*, 90:486–501, 2018.
- Graham, B. P., Kay, J. W., and Phillips, W. A. Context-sensitive processing in a model neocortical pyramidal cell with two sites of input integration. *Neural Computation*, 37(4):588–634, 2025.
- Granato, A., Phillips, W. A., Schulz, J. M., Suzuki, M., and Larkum, M. E. Dysfunctions of cellular context-sensitivity in neurodevelopmental learning disabilities. *Neuroscience & Biobehavioral Reviews*, pp. 105688, 2024.
- Greedy, Will, e. a. Single-phase deep learning in cortico-cortical networks. *Advances in Neural Information Processing Systems*, 2022.
- Guerguiev, J., Lillicrap, T., and Richards, B. Towards deep learning with segregated dendrites. *eLife*, 6:e22901, 12 2017. doi: 10.7554/eLife.22901.
- Häusser, M. Synaptic function: Dendritic democracy. *Current Biology*, 11(1):R10–R12, 2001. ISSN 0960-9822.
- Illing, B., Ventura, J., Bellec, G., and Gerstner, W. Local plasticity rules can learn deep representations using self-supervised contrastive predictions. *Advances in Neural Information Processing Systems*, 2022.
- Järnil Pérez, T. Exploring the cooperative abilities between homogeneous robotic arms: An explorative study of robotics and reinforcement learning, 2024.
- Kahneman, D. Thinking, fast and slow. *Farrar, Straus and Giroux*, 2011.
- Kastellakis, G., Silva, A. J., and Poirazi, P. Linking memories across time via neuronal and dendritic overlaps in model neurons with active dendrites. *Cell reports*, 17(6): 1491–1504, 2016.
- Kay, J., Floreano, D., and Phillips, W. A. Contextually guided unsupervised learning using local multivariate binary processors. *Neural Networks*, 11(1):117–140, 1998.
- Kay, J. W. and Phillips, W. A. Contextual modulation in mammalian neocortex is asymmetric. *Symmetry*, 12(5): 815, 2020.
- Kay, J. W., Schulz, J. M., and Phillips, W. A. A comparison of partial information decompositions using data from real and simulated layer 5b pyramidal cells. *Entropy*, 24 (8):1021, 2022.
- Kirkpatrick, J., Pascanu, R., Rabinowitz, N., Veness, J., Desjardins, G., Rusu, A. A., Milan, K., Quan, J., Ramalho, T., Grabska-Barwinska, A., et al. Overcoming catastrophic forgetting in neural networks. *Proceedings of the national academy of sciences*, 114(13):3521–3526, 2017.
- Körding, K. P. and König, P. Learning with two sites of synaptic integration. *Network: Computation in neural systems*, 11(1):25–39, 2000.
- Langley, P. Crafting papers on machine learning. In Langley, P. (ed.), *Proceedings of the 17th International Conference on Machine Learning (ICML 2000)*, pp. 1207–1216, Stanford, CA, 2000. Morgan Kaufmann.
- Larkum, M. A cellular mechanism for cortical associations: an organizing principle for the cerebral cortex. *Trends in neurosciences*, 36(3):141–151, 2013.
- Larkum, M. E. Are dendrites conceptually useful? *Neuroscience*, 489:4–14, 2022.
- Larkum, M. E., Zhu, J. J., and Sakmann, B. A new cellular mechanism for coupling inputs arriving at different cortical layers. *Nature*, 398(6725):338–341, 1999.
- Larkum, M. E., Petro, L. S., Sachdev, R. N., and Muckli, L. A perspective on cortical layering and layer-spanning neuronal elements. *Frontiers in neuroanatomy*, 12:56, 2018.
- LeCun, Y., Bengio, Y., and Hinton, G. Deep learning. *nature*, 521(7553):436–444, 2015.
- Limbacher, T. and Legenstein, R. Emergence of stable synaptic clusters on dendrites through synaptic rewiring. *Frontiers in computational neuroscience*, 14:57, 2020.
- Liu, Y., Tian, Y., Zhao, Y., Yu, H., Xie, L., Wang, Y., Ye, Q., Jiao, J., and Liu, Y. Vmamba: Visual state space model. *Advances in neural information processing systems*, 37: 103031–103063, 2024.
- Liu, Z., Lin, Y., Cao, Y., Hu, H., Wei, Y., Zhang, Z., Lin, S., and Guo, B. Swin transformer: Hierarchical vision transformer using shifted windows. In *Proceedings of the IEEE/CVF international conference on computer vision*, pp. 10012–10022, 2021.
- Major, G., Larkum, M. E., and Schiller, J. Active properties of neocortical pyramidal neuron dendrites. *Annual review of neuroscience*, 36:1–24, 2013.
- Marvan, T. and Phillips, W. A. Cellular mechanisms of cooperative context-sensitive predictive inference. *Current Research in Neurobiology*, pp. 6.100129, 2024.

- Marvan, T., Polák, M., Bachmann, T., and Phillips, W. A. Apical amplification—a cellular mechanism of conscious perception? *Neuroscience of consciousness*, 2021(2): niab036, 2021.
- Muckli, L., Petro, L., Abbatecola, C., Adeel, A., Bergmann, J., Deperrois, N., Destexhe, A., Kriegeskorte, N., Levelt, C., Maass, W., et al. The cortical microcircuitry of predictions and context—a multi-scale perspective. *Preprint at Zenodo*, 10, 2023.
- Nelson, A. D. and Bender, K. J. Dendritic integration dysfunction in neurodevelopmental disorders. *Developmental Neuroscience*, 43(3-4):201–221, 2021.
- Pagalos, M., Makarov, R., and Poirazi, P. Leveraging dendritic properties to advance machine learning and neuro-inspired computing. *arXiv preprint arXiv:2306.08007*, 2023.
- Parnas, J. and Sandsten, K. E. The phenomenological nature of schizophrenia and disorder of selfhood. *Schizophrenia Research*, 270:197–201, 2024.
- Parnas, J., Urfer-Parnas, A., and Stephensen, H. Double bookkeeping and schizophrenia spectrum: divided unified phenomenal consciousness. *European Archives of Psychiatry and Clinical Neuroscience*, 271:1513–1523, 2021.
- Pastorelli, E., Yegenoglu, A., Kolodziej, N., Wybo, W., Simula, F., Diaz, S., Storm, J. F., and Paolucci, P. S. Two-compartment neuronal spiking model expressing brain-state specific apical-amplification, -isolation and -drive regimes. *arXiv preprint arXiv:2311.06074*, 2023.
- Payeur, A., Guerguiev, J., Zenke, F., Richards, B. A., and Naud, R. Burst-dependent synaptic plasticity can coordinate learning in hierarchical circuits. *Nature neuroscience*, 24(7):1010–1019, 2021.
- Phillips, W. A. Cognitive functions of intracellular mechanisms for contextual amplification. *Brain and Cognition*, 112:39–53, 2017.
- Phillips, W. A. *The Cooperative Neuron: Cellular Foundations of Mental Life*. Oxford University Press, 2023.
- Phillips, W. A. and Silverstein, S. M. Convergence of biological and psychological perspectives on cognitive coordination in schizophrenia. *Behavioral and Brain Sciences*, 26(1):65–82, 2003.
- Phillips, W. A. and Silverstein, S. M. The coherent organization of mental life depends on mechanisms for context-sensitive gain-control that are impaired in schizophrenia. *Frontiers in Psychology*, 4:307, 2013.
- Phillips, W. A., Bachmann, T., Spratling, W., Muckli, L., Petro, L., and Zolnik, T. Cellular psychology: relating cognition to context-sensitive pyramidal cells. *Trends in Cognitive Sciences*, 29(1):28–40, 2024.
- Pienkos, E. Intersubjectivity and its role in schizophrenic experience. *The Humanistic Psychologist*, 43(2):194–209, 2015.
- Poirazi, P. and Papoutsi, A. Illuminating dendritic function with computational models. *Nature Reviews Neuroscience*, 21:1–19, 05 2020. doi: 10.1038/s41583-020-0301-7.
- Ramaswamy, S. and Markram, H. Anatomy and physiology of the thick-tufted layer 5 pyramidal neuron. *Frontiers in cellular neuroscience*, 9:233, 2015.
- Raza, M. and Adeel, A. An overlooked role of context-sensitive dendrites. *arXiv preprint arXiv:2408.11019*, 2024.
- Rumelhart, D. E., McClelland, J. L., Group, P. R., et al. *Parallel distributed processing, volume 1: Explorations in the microstructure of cognition: Foundations*. The MIT press, 1986.
- Sacramento, J., Ponte Costa, R., Bengio, Y., and Senn, W. Dendritic cortical microcircuits approximate the back-propagation algorithm. *Advances in neural information processing systems*, 31, 2018.
- Sass, L. and Pienkos, E. Faces of intersubjectivity: a phenomenological study of interpersonal experience in melancholia, mania, and schizophrenia. *Journal of Phenomenological Psychology*, 46(1):1–32, 2015.
- Schmid, D., Jarvers, C., and Neumann, H. Canonical circuit computations for computer vision. *Biological Cybernetics*, 117(4):299–329, 2023.
- Schulz, J. M., Kay, J. W., Bischofberger, J., and Larkum, M. E. Gaba b receptor-mediated regulation of dendrosomatic synergy in layer 5 pyramidal neurons. *Frontiers in cellular neuroscience*, 15:718413, 2021.
- Schuman, B., Dellal, S., Prönneke, A., Machold, R., and Rudy, B. Neocortical layer 1: An elegant solution to top-down and bottom-up integration. *Annual Review of Neuroscience*, 44(1):221–252, 2021. doi: 10.1146/annurev-neuro-100520-012117. PMID: 33730511.
- Selfridge, O. G. Pattern recognition and modern computers. In *Proceedings of the March 1-3, 1955, western joint computer conference*, pp. 91–93, 1955.
- Shin, J., Doron, G., and Larkum, M. Memories off the top of your head. *Science*, 374:538–539, 10 2021. doi: 10.1126/science.abk1859.

- Shine, J. M. Neuromodulatory influences on integration and segregation in the brain. *Trends in cognitive sciences*, 23 (7):572–583, 2019.
- Shine, J. M., Bissett, P. G., Bell, P. T., Koyejo, O., Balsters, J. H., Gorgolewski, K. J., Moodie, C. A., and Poldrack, R. A. The dynamics of functional brain networks: integrated network states during cognitive task performance. *Neuron*, 92(2):544–554, 2016.
- Shine, J. M., Breakspear, M., Bell, P. T., Ehgoetz Martens, K. A., Shine, R., Koyejo, O., Sporns, O., and Poldrack, R. A. Human cognition involves the dynamic integration of neural activity and neuromodulatory systems. *Nature neuroscience*, 22(2):289–296, 2019.
- Shine, J. M., Müller, E. J., Munn, B., Cabral, J., Moran, R. J., and Breakspear, M. Computational models link cellular mechanisms of neuromodulation to large-scale neural dynamics. *Nature neuroscience*, 24(6):765–776, 2021.
- Storm, J. F., Klink, P. C., Aru, J., Senn, W., Goebel, R., Pigorini, A., Avanzini, P., Vanduffel, W., Roelfsema, P. R., Massimini, M., et al. An integrative, multiscale view on neural theories of consciousness. *Neuron*, 112(10):1531–1552, 2024.
- Tang, Y. and Ha, D. The sensory neuron as a transformer: Permutation-invariant neural networks for reinforcement learning. *Advances in Neural Information Processing Systems*, 34:22574–22587, 2021.
- Touvron, H., Cord, M., Douze, M., Massa, F., Sablayrolles, A., and Jégou, H. Training data-efficient image transformers & distillation through attention. In *International conference on machine learning*, pp. 10347–10357. PMLR, 2021.
- Uhlhaas, P. J., Phillips, W. A., Schenkel, L. S., and Silverstein, S. M. Theory of mind and perceptual context-processing in schizophrenia. *Cognitive neuropsychiatry*, 11(4):416–436, 2006.
- Vaswani, A., Shazeer, N., Parmar, N., Uszkoreit, J., Jones, L., Gomez, A. N., Kaiser, Ł., and Polosukhin, I. Attention is all you need. *Advances in neural information processing systems*, 30, 2017.
- Vlaev, I. Local choices: Rationality and the contextuality of decision-making. *Brain sciences*, 8(1):8, 2018.
- Wei, J., Wang, X., Schuurmans, D., Bosma, M., Xia, F., Chi, E., Le, Q. V., Zhou, D., et al. Chain-of-thought prompting elicits reasoning in large language models. *Advances in neural information processing systems*, 35:24824–24837, 2022.
- Zenke, F., Poole, B., and Ganguli, S. Continual learning through synaptic intelligence. In *International conference on machine learning*, pp. 3987–3995. PMLR, 2017.
- Zhu, Y., Gao, T., Fan, L., Huang, S., Edmonds, M., Liu, H., Gao, F., Zhang, C., Qi, S., Wu, Y. N., et al. Dark, beyond deep: A paradigm shift to cognitive ai with humanlike common sense. *Engineering*, 6(3):310–345, 2020.



Figure 6. An example of “thinking fast and slow” as discussed in (Kahneman, 2011), illustrates how solving a riddle can involve combining rapid, intuitive processing in high-level perceptual state (fast thinking) with more deliberate, reflective refinement in the awake thought state (slow thinking).

A. Appendix

A.1. Varying Strengths of RF and CF Across Distinct Mental States: An Illustrative Example

This section illustrates how the strength of RF and CF inputs, and their interaction, varies across high-level perceptual processing and awake thought (imagination) states.

Read the ambiguous text in Figure 6 quickly at first, and then slowly (Kahneman, 2011; Selfridge, 1955; Rumelhart et al., 1986). When read quickly, our perception operates in a fast mode: automatic, pre-reflective, and anticipatory, neither too abstract nor too concrete (Parnas et al., 2021; Parnas & Sandsten, 2024; Blankenburg & Mishara, 2001). We are able to focus on relevant information and decode it with a reasonable degree of confidence and coherence within that context. This corresponds to high-level perceptual processing (Phillips et al., 2024): a state of being awake and conscious, characterized by basic, intuitive judgments sufficient for routine activities and everyday interactions, also known as common sense (Parnas et al., 2021; Parnas & Sandsten, 2024; Blankenburg & Mishara, 2001). In this state, the strength and interaction of both RF and CF inputs range from moderate to high (Mod-High), mediated by cholinergic, noradrenergic, and orexinergic systems (Phillips et al., 2024).

Now, if we slow down and take more time to interpret the information from different perspectives, we begin to perceive how identical characters can be interpreted differently depending on the context. For instance, consider the second character in both words in the first row, although visually identical, it is interpreted differently. Likewise, the first character in the second row and the second character in the third row are the same, yet each is perceived uniquely. This reflects a wakeful (imaginative) thought state (Phillips et al., 2024): a heightened state of awareness and imagination that involves deep⁵, slow, sequential, structured, deliberate, reflective, and well-justified judgments in context (Vlaev, 2018). In this case, the strength and interaction of RF and CF inputs range from high to maximal (High-Max), mediated by cholinergic, noradrenergic, and orexinergic pathways (Phillips et al., 2024).

Overall, the combination of high-level perceptual processing and awake thought helps us navigate uncertainty and explore deeper, more nuanced, and less obvious meanings, moving beyond the literal interpretations offered by attention alone.

A.2. From 20th-century point neurons to 21st-century two-point neurons

The brain is made up of billions of neurons, most receiving input from thousands of other neurons (Azevedo et al., 2009). In 20th-century, neurally-inspired AI researchers assumed that neurons summed all their inputs to generate an output, a concept of point neurons (PNs), on which most current brain theories and AI systems are based (Häusser, 2001; LeCun et al., 2015). The neuroscience of the 21st century (Larkum et al., 1999; Phillips, 2017; 2023; Larkum, 2013; Major et al., 2013; Ramaswamy & Markram, 2015; Larkum, 2022; Adeel, 2020; Körding & König, 2000; Schuman et al., 2021; Poirazi & Papoutsis, 2020; Larkum et al., 2018; Shine et al., 2016; 2019; Shine, 2019; Shine et al., 2021; Schulz et al., 2021; Kay & Phillips, 2020; Kay et al., 2022) has revealed that some neurons, particularly some pyramidal neurons, have two points of input integration, often referred to as TPNs. They combine information from the external environment (RF) at one point (basal dendrites) and internal world (CF) at another (apical dendrites).

Recent studies have concluded that the coupling of RF and CF is the hallmark of conscious processing (Aru et al., 2021;

⁵Deep refers to the complex integration of diverse CFs at the cellular level, enabled by TPNs.

Storm et al., 2024; Marvan et al., 2021). This coupling does not occur under anesthesia (i.e., they are decoupled). In the conscious state, the gate within the cells is open that allows CF from a wide range of cortical and subcortical sources to propagate and evolve in the thalamocortical and corticocortical loops (Aru et al., 2021). The CF arriving from cortical and subcortical sources, and beyond, include feedback (FB) (reward), lateral intra-regional loops, and interactions between neocortical cells and the higher-order thalamus, and beyond (Phillips et al., 2024). These contextual signals can be represented as FB, proximal (P), distal (D), and universal (U) (Adeel, 2020; Adeel et al., 2023a; Muckli et al., 2023). The coupling between CF and RF enables the propagation of coherent information streams. This does not occur in an unconscious state.

Coherent dendritic integration in TPNs occurs extensively across the cortical sheet, enhancing both individual neuronal complexity (Aru et al., 2021; Bachmann et al., 2020) and the capacity for moment-to-moment cooperation. This enables neurons to selectively transmit coherent thoughts while suppressing conflicting ones, ultimately promoting harmony and consistency in brain-wide activity (Phillips, 2023).

Dysfunctional interactions between RF and CF inputs are linked to children with intellectual learning disabilities or significantly lower reasoning capabilities (Nelson & Bender, 2021; Granato et al., 2024). Patients with cognitive or perceptual conditions such as psychosis⁶ lack this balanced interaction between RF and CF, and struggle to focus on relevant information within a specific context (Pienkos, 2015; Parnas et al., 2021; Parnas & Sandsten, 2024; Sass & Pienkos, 2015; Blankenburg & Mishara, 2001; Zhu et al., 2020).

A.3. Extended Background

Inspired by TPNs, computational neuroscientists have proposed various biologically plausible learning algorithms, including the recent burst-dependent synaptic plasticity (BDSP) (Payeur et al., 2021; Greedy, 2022), which distinguishes between a single spike and a burst of spikes. It uses the top-down (apical) zone of the TPN to receive FB signals (bursting rate b) from higher perceptual levels as CF. The difference between the instantaneous and moving average of b is multiplied by the event rate (e) or RF to update weights (W). BDSP approximates loss-function gradients similar to backpropagation and performs comparably on complex image patterns, addressing the credit assignment problem effectively. However, BDSP and similar algorithms (Guerguiev et al., 2017; Sacramento et al., 2018; Illing et al., 2022; Greedy, 2022; Zenke et al., 2017; Kirkpatrick et al., 2017; Kastellakis et al., 2016; Bono & Clopath, 2017; Limbacher & Legenstein, 2020) focus mainly on apical inputs for learning. While their learning is TPN-inspired, their processing is not.

In contrast, there is ample neurobiological evidence suggesting that context serves as a modulatory factor (Marvan & Phillips, 2024; Schulz et al., 2021; Kay & Phillips, 2020; Kay et al., 2022; Phillips, 2023). Neurophysiologists have proposed several biologically plausible asynchronous modulatory (MOD) transfer functions (Schulz et al., 2021; Kay & Phillips, 2020; Kay et al., 2022; Phillips, 2023; Schmid et al., 2023) and their latest iterations (Pastorelli et al., 2023; Graham et al., 2025); however, whether there are many applications in which deep neural nets (DNNs) inspired by these transfer functions can outperform Point Neurons (PNs) (Adeel et al., 2023a)-driven DNNs is yet to be seen. Below are these alternative well-established TPNs-inspired asynchronous MOD functions (Kay et al., 1998; Phillips, 2023). In these modulatory transfer functions (T_M) eq (2-5), R is the driving force.

$$T_{M1}(R, C) = \frac{1}{2}R(1 + \exp(RC)) \quad (16)$$

$$T_{M2}(R, C) = R + RC \quad (17)$$

$$T_{M3}(R, C) = R(1 + \tanh(RC)) \quad (18)$$

$$T_{M4}(R, C) = R(2^{RC}) \quad (19)$$

Recently a new TPN MOD function (Adeel et al., 2023a; Muckli et al., 2023; Raza & Adeel, 2024) incorporated not only FB from higher perceptual levels but also simultaneous events across hierarchies while processing FF information (Aru et al., 2021; Bachmann et al., 2020; Shin et al., 2021; Adeel et al., 2023a; Muckli et al., 2023). This MOD function uses CF to split the RF into coherent and incoherent streams at the cellular level, recombining only the coherent ones. The MOD function assigns greater weight to CF, amplifying or attenuating RF based on CF's strength.

Recent computational results with convolutional neural nets (CNNs) (Adeel et al., 2023a) have shown that TPNs-inspired

⁶The individuals whose ability to distinguish between imagination and reality is seriously impaired, for example, believing that imagined voices are real (Phillips & Silverstein, 2003; Uhlhaas et al., 2006; Phillips & Silverstein, 2013).

CNN with this MOD function minimizes the transmission of large amounts of conflicting FF information to higher perceptual levels, greatly reducing (by orders of magnitude) the number of neurons required to process large amounts of heterogeneous real-world audio-visual data compared to PN-inspired CNNs (Adeel et al., 2023a). The most recent study in cellular psychology (Phillips et al., 2024) links these types of MOD functions to apical drive (AD), which is utilized in Co⁴.

A.4. Bursting probabilities under distinct mental-state-dependent processing regimes

Slow-wave sleep/ AI and Apical Cooperation (AC):

During SW sleep, apical input is functionally disconnected, and internal belief dynamics remain largely decoupled from sensory evidence. However, in this lowest-coherence regime, under low R and low C inputs, salience emerges only when both basal and apical inputs coincide, corresponding to minimal bursting probability in apical cooperation, such that:

$$\begin{aligned} P_2^{LL}(b, a) &= P_{1b}(b) P_{2a}(a) \\ &\equiv g^{LL}(b, a) \end{aligned} \quad (20)$$

Here, $P_2^{LL}(b, a)$ is the bursting probability under low basal (b) and low apical (a) inputs. $P_{1b}(b)$ is the probability of an initial somatic spike from basal input alone, and $P_{2a}(a)$ is the conditional contribution of apical input leading to a second spike (burst) (Graham et al., 2025).

The reinterpreted MOD dynamics are defined as: $\text{MOD}(R, C) = g(R, C)$.

Apical Amplification:

$$\begin{aligned} P_2^{HL}(b, a) &= P_{1b}(b) P_{2b}(b) \\ &\quad + P_2^{LL}(b, a) [1 - P_{2b}(b)] \\ &\equiv f_b(b) + g^{HL}(b, a) \end{aligned} \quad (21)$$

$P_2^{HL}(b, a)$ represents bursting under high basal and low apical input. $P_{2b}(b)$ is the burst probability from basal input alone (Graham et al., 2025).

The reinterpreted MOD dynamics are defined as: $\text{MOD}(R, C) = f(R) + g(R, C)$.

Apical Drive:

$$\begin{aligned} P_2^{LH}(b, a) &= P_{2a}^H(a) \\ &\quad + P_2^{LL}(b, a) [1 - P_{2a}^H(a)] \\ &\equiv f_a(a) + g^{LH}(b, a) \end{aligned} \quad (22)$$

$P_2^{LH}(b, a)$ is the bursting probability under low basal and high apical input. $P_{2a}^H(a)$ denotes the probability that apical input alone produces a spike (Graham et al., 2025).

The reinterpreted MOD dynamics are defined as: $\text{MOD}(R, C) = f(C) + g(R, C)$.

Apical Drive + Awake:

$$\begin{aligned} P_2^{HH}(b, a) &= P_{2a}^H(a) \\ &\quad + P_2^{HL}(b, a) [1 - P_{2a}^H(a)] \\ &\equiv f_a(a) + f_b(b) + g^{HH}(b, a) \end{aligned} \quad (23)$$

$P_2^{HH}(b, a)$ is the bursting probability under high basal and high apical input. In this regime, both sources can independently initiate bursting, and their interaction further enhances amplification (Graham et al., 2025).

The reinterpreted MOD dynamics are defined as: $\text{MOD}(R, C) = f(R) + f(C) + g(R, C)$.

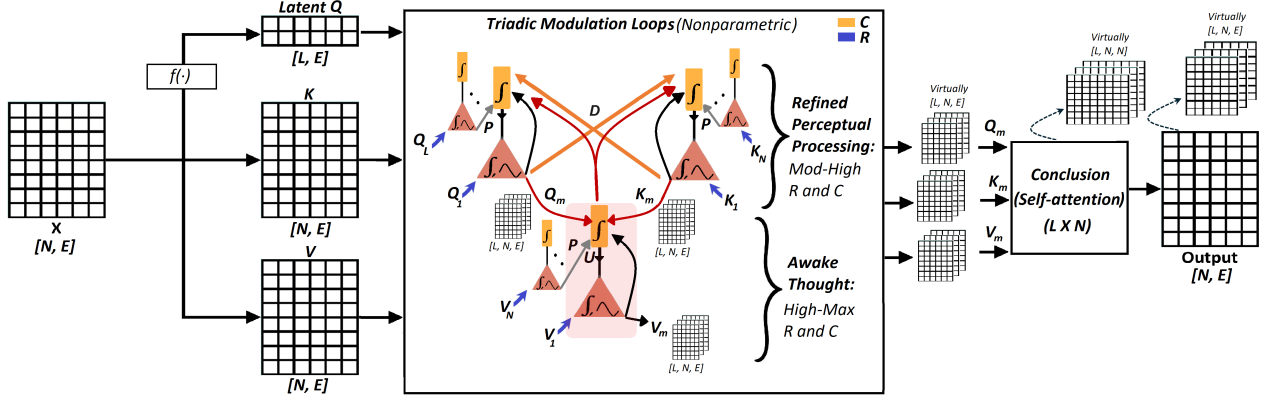


Figure 7. Co^4 basic architecture: latent Q , K , and V tokens evolve via TPN-like circuits and triadic modulation under distal, proximal, and universal context. Enables scalable, context-sensitive reasoning at an approximate cost of $\mathcal{O}(N)$.

All component functions $P_1^b(b)$, $P_2^a(a)$, $P_2^b(b)$, and $P_{2a}^H(a)$ are sigmoidal functions of stimulus amplitudes (Graham et al., 2025).

A.5. Co^4 basic architecture

Co^4 architecture: N denotes the number of input tokens, and each token has an embedding dimension of E . Q_1, Q_2, \dots, Q_L represent the latent query tokens input to the associated Q-TPNs. K_1, K_2, \dots, K_N represent the Key tokens input to the associated K-TPNs. V_1, V_2, \dots, V_N represent the Value tokens input to the associated V-TPNs. This configuration forms part of the “seeing” state (i.e., sensory processing). In the “seeing as” state (i.e., perceptual and interpretive state), triadic modulation loops among questions (Q), clues (keys, K), and hypotheses (values, V) are executed through distal (D) and universal (U) contexts. Proximal (P) context represents normalization via information from neighboring neurons in the same population, including the prior information from the same neuron. The TPNs associated with Q , K , and V are assumed to be analogous to three subtypes of pyramidal neurons, although their exact correspondence to neurobiologically distinguished subtypes is still under investigation. Through varying states of mind, high-level perceptual processing and wakeful thought, diverse, parallel reasoning chains are enabled. This mechanism incurs a computational cost of $\mathcal{O}(N \cdot L)$, where L is a small fraction of the input length, making the overall cost approximately $\mathcal{O}(N)$. The triadic modulation loops, based on element-wise operations, add a nominal cost of $L \cdot N \cdot E$, which is significantly lower than that of the feedforward residual network used in standard Transformer blocks, a component Co^4 does not require. Co^4 can be viewed as a parallel, representation-level, silent yet deep form of Chain-of-Thought (CoT) reasoning (Wei et al., 2022) (a quiet mind), enabling multi-perspective inference without requiring sequential token-level generation, much like the brain’s cortico-thalamic modulation (Aru et al., 2021; Phillips et al., 2024; Storm et al., 2024).

A.6. Computational complexity

Basic Co^4 has a computational complexity of

$$\mathcal{O}(l \cdot N + \alpha)$$

where N is the number of input tokens (patches or words), l is the number of latent tokens, and α accounts for additional element-wise operations. Instead of full attention between all N tokens,

$$\Rightarrow \mathcal{O}(N^2),$$

the model, similar to latent Transformers (Bi et al., 2024), restricts this to $l \times N$ interactions where l is a small fraction of the input length N i.e., $l \ll N$,

$$\Rightarrow \mathcal{O}(N \cdot l) \approx \mathcal{O}(N)$$

The element-wise operations in triadic modulation loops are significantly less expensive than matrix multiplications and lower than that of the FF residual network used in standard Transformer blocks, which Co^4 does not require. Co^4 scales linearly with input length, in contrast to the quadratic scaling in standard Transformers. For more explicit complexity

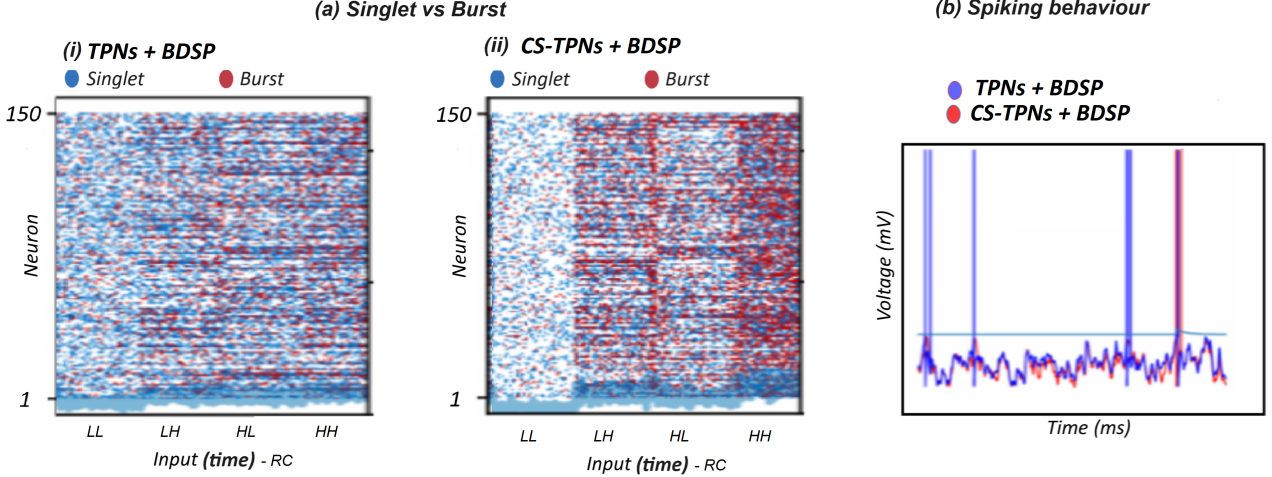


Figure 8. (a) Raster plots for 150 neurons. (i) standard TPNs + BDSP (ii) and context-sensitive (CS)-TPNs + BDSP with cooperative $MOD(R, C)$ dynamics. In CS-TPNs, a clear distinction in bursting probability is observed as the inputs transition from low–low (LL) to high–high (HH), corresponding to input combinations 00, 01, 10, and 11. (b) CS-TPNs fire substantially less frequently than TPNs alone and exhibit bursting primarily when R and C inputs are coherent.

analysis, the dominant MAC (multiply–accumulate) operations in standard Transformer model are approximated as:

$$\text{MACs}_{\text{standard}} \approx L \left(P E^2 + P^2 E \right)$$

Where E , P , and L represent the embedding dimension, number of tokens (or patches), and the number of layers, respectively. The term $P E^2$ represents the cost of the Q, K, V projections plus the FF network. The term $P^2 E$ is due to the self–attention mechanism, which scales quadratically with P .

For the Co^4 model, the dominant MAC operations are approximated as:

$$\text{MACs}_{\text{Co}^4} \approx L \left(L_q E^2 + P E^2 + L_q P E \right)$$

L_q represent the number of latent (query) tokens (with $L_q \ll P$). The term $L_q E^2$ arises from projecting the L_q latent queries. The term $P E^2$ corresponds to the key and value projections. The term $L_q P E$ reflects the cost of triadic modulation loops (emulating high-level perceptual processing and wakeful thought states), which scales linearly with P since L_q is small.

For the scaled Co^4 , the dominant MAC operations can be approximated as

$$\text{MACs}_{\text{Co}^4} \approx L \left(N E^2 + N E + N \log k + k^2 E \right), \quad (24)$$

where k denotes the number of selected tokens in the Top- k aggregation step. The term $N E^2$ corresponds to the projection cost for computing queries, keys, and values. The term $N E$ arises from the element-wise triadic modulation between the latent token and the patch tokens. The term $N \log k$ reflects the complexity of Top- k token selection, which, under the constraint $k \sim N^{1/2}$, scales sub-quadratically and behaves linearly in practice due to the small constant k . Finally, the term $k^2 E$ accounts for the attention computation restricted to the reduced latent-enhanced token set, which remains negligible since $k \ll N$.

A.7. Bursting probability dynamics across varying strengths of R and C

A variation of Eq. 12 was used in burst-dependent synaptic plasticity (BDSP) spiking simulations (Raza & Adeel, 2024). In these simulations, the strengths of the receptive (R) and contextual (C) inputs were varied across four regimes: low–low

(LL), low–high (LH), high–low (HL), and high–high (HH). As shown in Fig. 8, the resulting bursting probability increases consistently as the system transitions from LL to HH, reflecting the increasing coherence between contextual and FF signals.

$$\text{Mod}(I_s, I_c, I_u) = I_s + I_c(0.1 + |I_s|) + I_u I_c(2 + |I_s|) \quad (25)$$

Here I_s , I_c , and I_u denote the somatic (basal) current, the integrated contextual current, and the synergistic (universal) context current, respectively.

Following the formulation in (Payeur et al., 2021), the somatic membrane potential dynamics and apical dendritic modulation of context-sensitive pyramidal neurons (CS-TPNs) can be described by the following simplified differential equations (Eqs. 26–27):

$$\dot{V}_s = \frac{1}{\tau_s}(V_s - E_L) + \frac{1}{C_s}\text{Mod}(I_s, I_c, I_u) - \frac{1}{C_s}w_s \quad (26)$$

$$\dot{w}_s = -\frac{1}{\tau_{ws}}w_s + bS(t) \quad (27)$$

where V_s represents the membrane potential of the somatic compartment, $\tau_s = 16$ ms is the membrane time constant, $C_s = 370$ pF is the membrane capacitance, and $E_L = -70$ mV is the leak reversal potential. The variable w_s denotes a spike-triggered adaptation current.

The total current applied to the soma is given by $\text{Mod}(I_s, I_c, I_u)$, which represents basal current I_s modulated by contextual input I_c together with synergistic interaction components I_u . The basal current I_s corresponds to integrated synaptic inputs (including receptive excitatory and inhibitory inputs) together with basal noise. The contextual current I_c reflects the combined influence of proximal and distal contextual signals as well as feedback error signals, together with dendritic noise. The synergistic term I_u captures the extracted cooperative feedforward–contextual interaction components.

The adaptation variable w_s evolves according to Eq. 27, where $S(t)$ denotes the spike train of the neuron and $b = 200$ determines the strength of spike-triggered adaptation. A spike is emitted whenever V_s crosses a dynamic threshold of -50 mV. Following a spike, the threshold is increased by 2 mV and decays back to -50 mV with a time constant of 27 ms. After each spike, the membrane potential is reset to the resting voltage $V_r = -70$ mV. These parameter values follow those reported in (Payeur et al., 2021).

A more detailed analysis of these spiking simulations can be found in (Raza & Adeel, 2024).

A.8. Significance Statement and Future Directions

While the development of human-like AI raises important ethical considerations, the evidence presented here suggests that awake imaginative thought may be grounded in cooperative neural processes shaped by evolution (Bregman, 2020; Phillips, 2023). In addition to demonstrating fast and economical learning by emulating awake imaginative regimes, the present investigation suggests that context is actively constructed from available information to support internal hypotheses. When early internal inferences are misleading, convergence to accurate conclusions may require substantially more time or may fail altogether under constrained computational resources. This motivates the hypothesis that effective awareness, in a computational sense, arises from the capacity to iteratively evolve coherent latent queries, clues, and hypotheses in alignment with incoming evidence. Without such alignment, perceptual representations may become unstable or misleading.

These observations raise a broader question: whether the cellular mechanisms underlying context-sensitive integration in higher mammals can inform principled models of common-sense and imaginative reasoning, and thereby guide the design of future AI systems that are more ethical, efficient, robust, and context-aware. Overall, such biologically grounded mechanisms may help advance AI beyond conventional passive information processing toward more coherent, context-sensitive, and real understanding grounded in internal–external representational alignment.